Electronic Supplementary Material (ESI) for Energy & Environmental Science.

Supplementary information

Specific carbon/iodide interactions in electrochemical capacitors monitored by EQCM technique

Anetta Platek-Mielczarek, Elzbieta Frackowiak*, Krzysztof Fic*

Institute of Chemistry and Technical Electrochemistry, Poznan University of Technology, Berdychowo 4, Poznan 60-965, Poland

*corresponding authors: elzbieta.frackowiak@put.poznan.pl, krzysztof.fic@put.poznan.pl

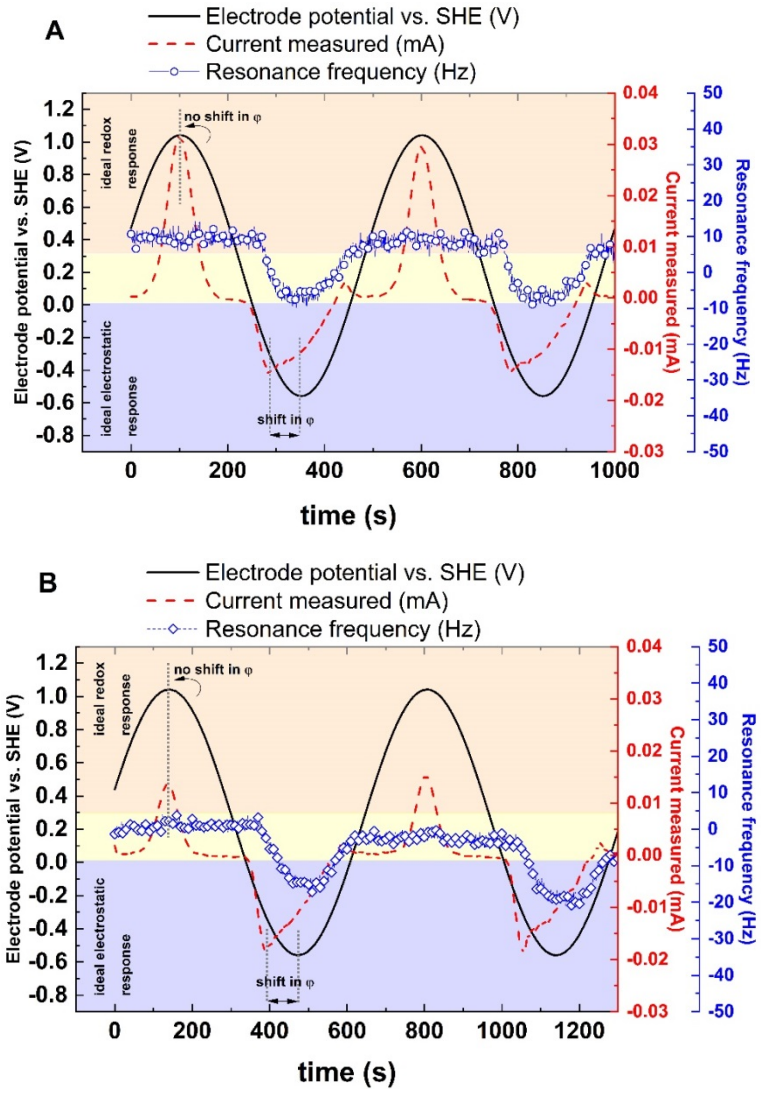

Fig. S1 LASV profiles (0.1 mol·L^{-1} RbI) for: (A) YP-50F carbon coating; (B) bare current collector

The redox contribution of the 0.1 mol·L^{-1} RbI electrolytic solution has been proven by a large-amplitude sinusoidal voltammetry (LASV) experiment performed with a YP-50F carbon electrode (**Fig. S1A)** and a pure metallic current collector (**Fig. S1B)**. The same current and frequency change patterns are observed. When pure electrostatic contribution is assumed from the current response during cyclic voltammetry (rectangular shape of the curve), the potential and current as a function of time are shifted in phase (blue zone corresponds to ideal electrostatic attractions in accordance with **Fig. 4**). Moreover, one may notice that the mass change is also shifted from the current response, which may cause a delay in the ongoing phenomena description. Thus, the mass and potential are in the same time phase. It might be seen that the potential and current are in the same phase as the redox reaction proceeds (the red zone corresponds to the ideal redox response).

A summary of Rb^+ adsorption/desorption pure electrostatic attractions is predicted and proven by LASV experiments at potentials < 0 V *vs.* SHE. In the anion adsorption/desorption zone, the redox reaction of iodide is present at potentials > 0.3 V *vs.* SHE.

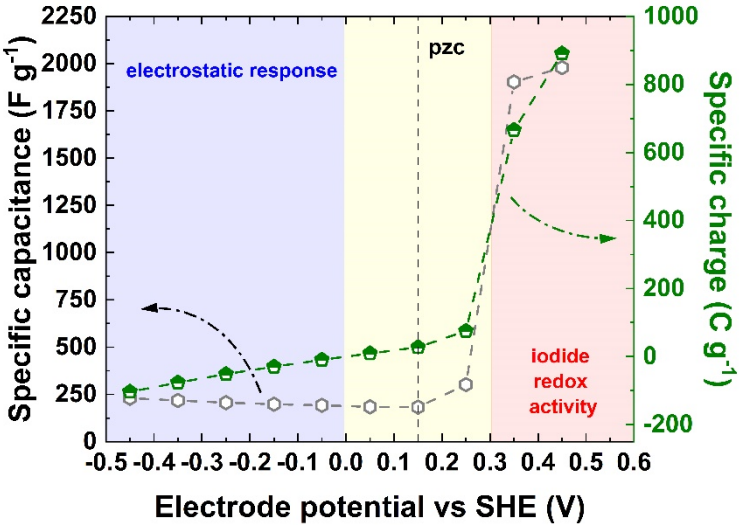

Fig. S2 Determination of the pzc from electrochemical impedance spectroscopy measurements (electrolyte: 0.1 mol·L^{-1} RbI, carbon: YP-50F)

The point of zero charge (pzc) was determined by impedance spectroscopy at various potentials using a 3-electrode Swagelok® cell (Fig. S2). The calculated specific capacitance at 10 mHz was plotted against the potential applied, and the minimum value could be easily distinguished, i.e., 0.150 V *vs.* SHE. Such observations have been double-checked by cyclic voltammetry with a wide potential range, where the minimum capacitance has been determined. Moreover, it is valuable to consider that the pzc may only be identified by the current or capacitance curve *vs.* applied potential. While considering a specific charge, it is impossible to determine the minimal value because it is strictly correlated with a potential value and sign. However, one may note that for redox-based systems or pseudocapacitive contributions, charge-based metrics might be more relevant than capacitance. We do agree with this statement; however, as our experiments are based on voltammetry techniques in order to compare systems between themselves, it is more relevant to consider capacitance.

Tab. S1 Textural properties of studied activated carbons: YP-50F, YP-80F and Kynol 507-20

Textural properties	YP-50F		YP-80F		Kynol 507-20
	Powder	Electrode material	Powder	Electrode material	Carbon fabric
S_{BET}, $m^2 g^{-1}$	1762	1423	2087	1771	1841
S_{DFT}, $m^2 g^{-1}$	1553	1251	1715	1459	1697
V_{TOTAL}, $cm^3 g^{-1}$	0.75	0.61	1.06	0.90	0.69
V_{MICRO}, $cm^3 g^{-1}$	0.67	0.54	0.80	0.68	0.69

Comparison of textural properties of selected carbon materials is shown in Table S1. YP-50F, YP-80F and Kynol® 507-20 are representative of activated carbons with developed specific surface area, i.e., S_{BET}>1500 $m^2 g^{-1}$. YP-80F contains more micropores and also mesopores (**Fig. S3**), what correlates well with higher specific surface area (both S_{BET} and S_{DFT}) found for powder state and electrode material comparing to YP-50F. Thus, it is assumed that for this material more complex ion phenomena during electrochemical operation may occur.

Two activated carbons with different textural properties (YP-50F and YP-80F) have been selected for EQCM studies to show that observed energy storage mechanism is universal for all microporous ACs operating in iodide-based electrolytic solutions. Moreover, in order to prove this concept, the long-term aging tests have been performed with Kynol® 507-20 carbon fabric electrodes at elevated voltages (**Fig. S10**). Despite self-standing character of Kynol® 507-20, fixed thickness made implementation of this material in the EQCM study impossible.

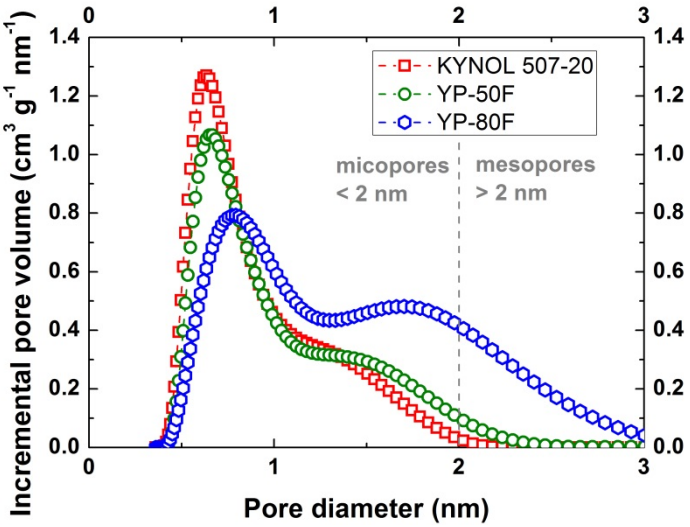

Fig. S3 Pore size distribution of powder state activated carbon: YP-50F, YP-80F and carbon textile Kynol 507-20

Calculation of the theoretical capacity of the YP-50F material

The theoretical capacity of the material was calculated taking into account Avogadro's number, N_A= $6.02214076 \cdot 10^{23}$ mol^{-1}, which describes the number of species in 1 mol of matter.

Therefore, considering the 400 μL volume of the electrolytic solution with a rubidium iodide salt concentration of 0.1 $mol \cdot L^{-1}$, the amount of Rb^+ is 0.00004 mol, the same as that of I^-. This number of moles implies $2.408856304 \cdot 10^{19}$ species. By knowing this value and assuming an ideal, spherical shape of ions, the volume occupied by them can be calculated.

All data necessary for performing these calculations are presented in **Tab. S2**.

Tab. S2 Data for theoretical calculations:

	Rb^+	**K^+**	**Na^+**
Radius [nm]	0.164	0.138	0.107
Volume of 1 species, $\cdot 10^{-23}$ [cm^3]	1.848	1.101	0.513
Coating mass [μg]	60	85	78
Volume of pores $\geqslant$ ion diameter according to mass coating [cm^3]	0.0012	0.0017	0.0013
Maximal number of ions in the pores, $\cdot 10^{20}$	0.6602	1.5836	2.5979

Thus, the pores are capable of storing all ions; i.e., in the case of Rb^+, it is $0.6602 \cdot 10^{20}$ of ions, which might fill the pore volume, whereas in the electrolytic solution, it is $0.2409 \cdot 10^{20}$ ions.

If all of the ions adsorb on the surface of the material, the maximal mass change recorded for Rb^+, K^+ and Na^+ should be 3400 μg, 1560 μg, and 920 μg, respectively.

Knowing the mass change recorded by EQCM on the level of micrograms (**Fig. 3**, **Fig. 5**, **Fig. 7**), one may calculate that only 2-5% of the theoretical capacity of the material

is used. However, from the cell construction point of view, it should be highlighted that in a full device, only the electrode pore volume needs to be filled with electrolytic solution. In 3-electrode studies, excess electrolyte is desirable and required in order to avoid any limitations during electrochemical tests. Moreover, for various electrolyte concentrations, both the number of ions present in the system and (what we consider a very important factor) the number of water molecules change.

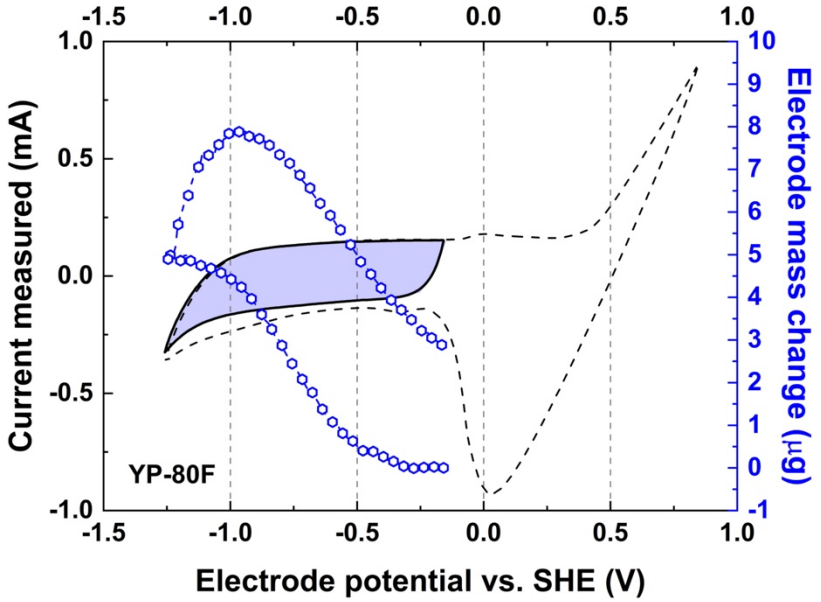

Fig. S4 Mass change recorded (electrode: YP-80F; electrolyte: 0.1 mol·L^{-1} RbI) during a cyclic voltammetry scan at 5 mV·s^{-1} presented with the current measured

The data from cyclic voltammetry simultaneously recorded with the electrode frequency change (calculated to the mass change) presented in **Fig. S4** for YP-80F activated carbon coincides with Fig. 2A for YP-50F. The same trend of the mass change *versus* potential curve is observed for both carbons. Hysteresis loop is even more pronounced in case of more porous carbon, i.e., YP-80F; this suggests that the hypothesis about ions confinement is valid. Hysteresis loop on the electrode mass change curve is not closed as the desorption process was experimentally limited - not fully conducted, i.e., vertex potential range was set to be lower than -0.1 V *vs.* SHE in order to split capacitive performance with redox activity - what can be seen in the cyclic voltammetry presented in a wide potential range. When YP-80F carbon is applied as an electrode material, potential shift of iodide/iodine redox activity and its high current response especially during the reduction process are observed.

Calculating the slope of the mass to charge plot for YP-80F it has been noticed that the species responsible for ion fluxes during negative polarization are heavier *i.e.*, $[Rb^+]\cdot[15H_2O]$, than in case of YP-50F electrode. Thus, qualitatively the cation adsorption process – its

mechanism, may be considered as the same when rubidium iodide aqueous solutions is in the vicinity of polarized activated carbon surface. While considering this process quantitatively, ion fluxes firmly depend on the textural properties of electrode material, what stays in the perfect agreement with other literature data.

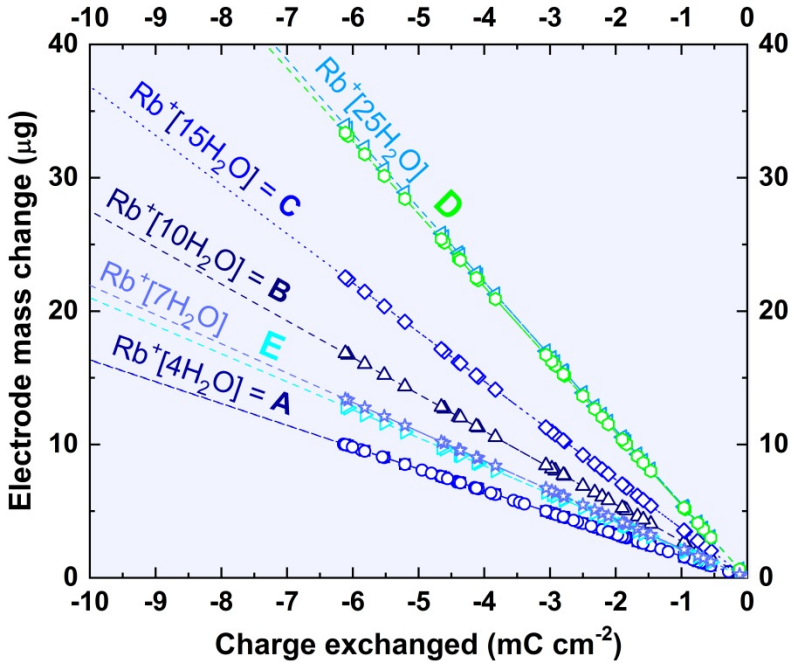

Fig. S5 Mass-charge plot for cation adsorption on YP-50F and YP-80F carbon recorded in 0.1 mol·L^{-1} and 0.01 mol·L^{-1} RbI. Experimentally recorded mass changes for various system configuration are represented by A-E lines. A: YP-50F:PVdF 60:40 + 0.1 mol·L^{-1}; B: YP-50F:PVdF 60:40 + 0.01 mol·L^{-1}; C: YP-80F:PVdF 60:40 + 0.1 mol·L^{-1}; D: YP-80F:PVdF 60:40 + 0.01 mol·L^{-1}; E: YP-50F:PVdF 80:20 + 0.01 mol·L^{-1}

Fig. S5 summarized cation fluxes during negative polarization for various studied systems: YP-50F and YP-80F, 0.1 mol·L^{-1} and 0.01 mol·L^{-1} RbI, 60:40 and 80:20 (w/w) coating composition. Recorded mass change varies in a wide range (from ca. 158 μg up to 535 μg); thus, the plot is presented in a narrow charge scale in order to better visualize the relevant lines. Mass *vs.* charge plot indicates that electrolytic solution dissolution favors solvation process, as more free solvent molecules are present in the electrolyte volume. When YP-50F was applied as electrode material 4 molecules of water are found in the solvation shell of Rb^+ cation in case of 0.1 mol · L^{-1} concentration (**line A**), whereas for 0.01 mol · L^{-1} solution it is 10 (**line B**). A good agreement with this data has been found when YP-80F was used as electrode

material. In 0.1 mol·L^{-1} RbI solution 15 molecules of water surrounds Rb^+ cation (**line C**). In 0.01 mol·L^{-1} this number changes up to 25 molecules (**line D**). For both ACs, taking these results into account it can be stated that decreasing the salt concentration in water, the number of solvent molecules creating solvation shell increases. It results from greater availability of water molecules in the electrolyte.

Moreover, what is important to consider is the fact that Rb^+ in the vicinity of more porous electrode material (*i.e.*, YP-80F) is solvated by greater number of water molecules, when the same electrolytic solution concentration is studied. For 0.1 mol · L^{-1} RbI solution solvation number of rubidium varies from 4 (**line A**) to 15 (**line C**) for YP-50F and YP-80F, respectively. When lower electrolyte concentration is applied, i.e., 0.01 mol·L^{-1}, as already deliberated, higher solvation number has been found for the cation according to described trend. More porous carbon allows ion fluxes richer in number of species/ions to occur. For YP-50F $Rb^+ \cdot [10H_2O]$ (**line B**) has been found, compared to YP-80F $Rb^+ \cdot [25H_2O]$ (**line D**).

Interesting conclusion can be drawn from comparison of ionic fluxes found for various carbon coating composition YP-50F:PVdF, i.e., 60:40 (w/w) (**line B**) or 80:20 (w/w) (**line E**) with 0.01 mol·L^{-1} solution. It demonstrates that amount of carbon in the electrode composite plays a minor role, considering the composition of the ionic flux (ratio of cation number to water molecules). For both examined carbon coatings on the basis of the same AC (YP-50F) similar solvation number of Rb^+ cation has been found: 10 for 60:40 and 7 for 80:20.

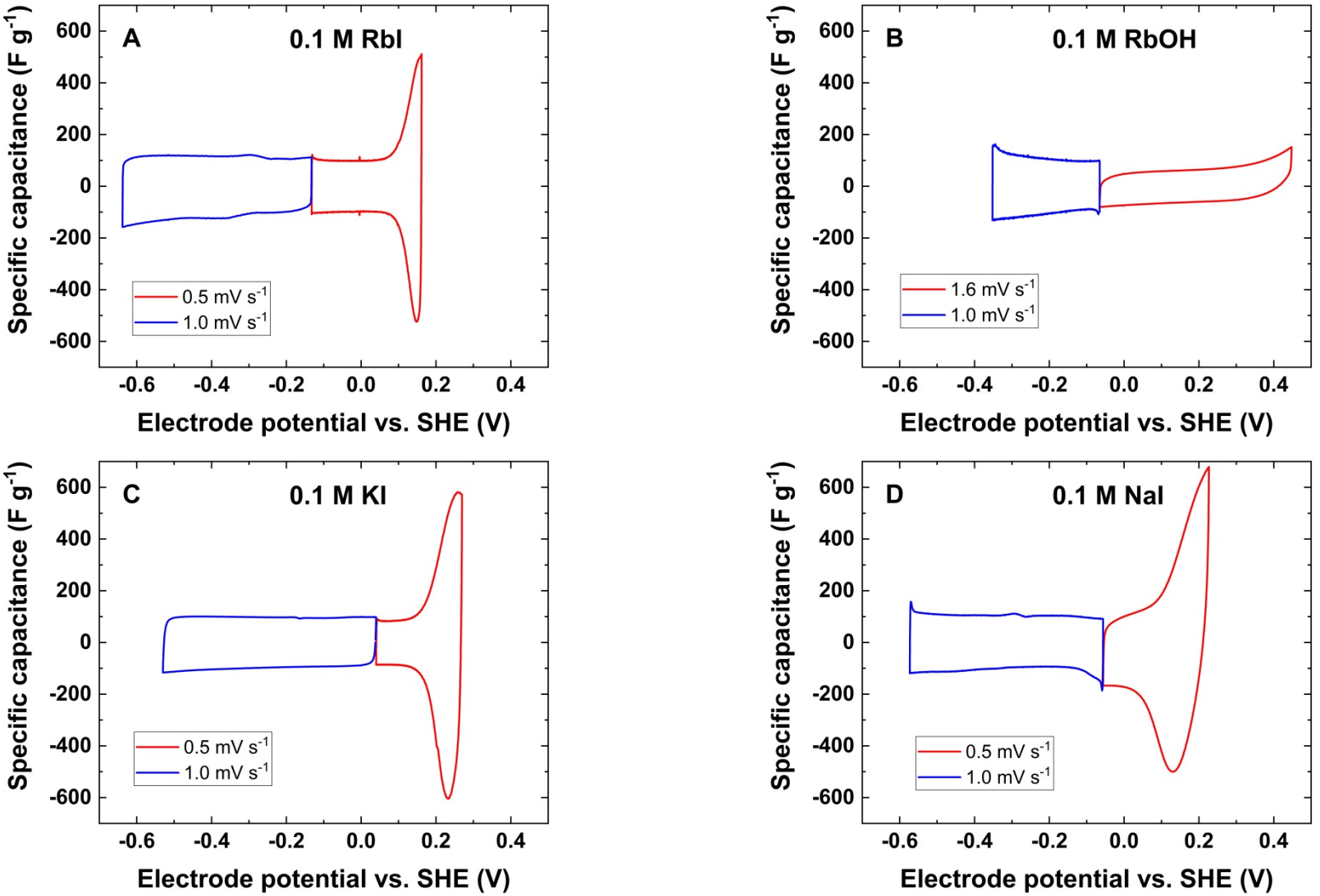

Fig. S6 Cyclic voltammetry profiles in symmetric Swagelok® cells (electrode: YP-50F; electrolytes: 0.1 mol·L^{-1}): A) RbI; B) RbOH; C) KI; and D) NaI

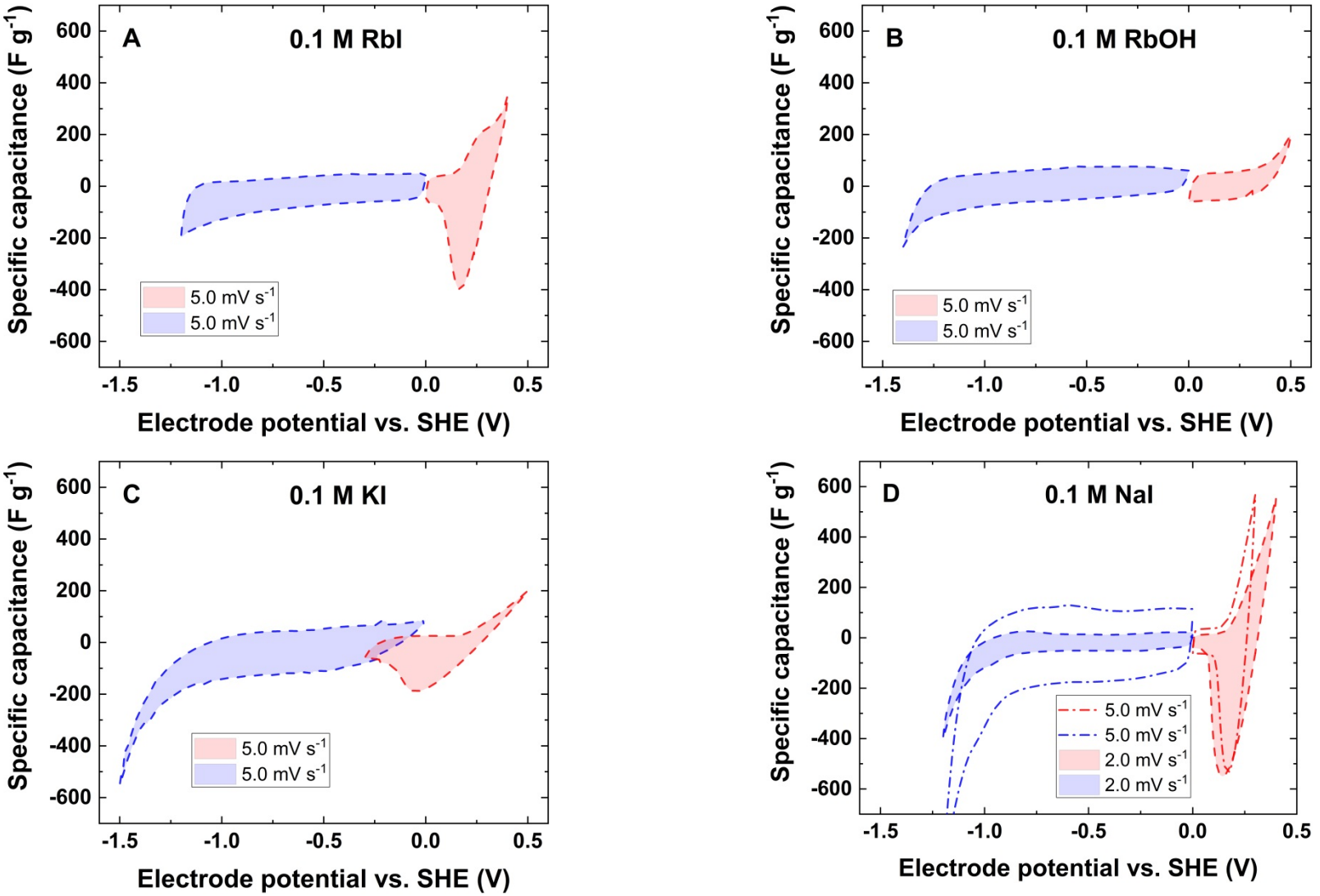

Fig. S7 Cyclic voltammetry profiles in EQCM cells (electrode: YP-50F; electrolytes: 0.1 mol·L^{-1}): A) RbI; B) RbOH; C) KI; D) NaI

Cyclic voltammetry profiles with a 0.8 V voltage range using symmetric Swagelok® cells in different electrolytes are presented in **Fig. S6**. Potentials for each electrode were designated from constant current charging/discharging at 0.1 $A \cdot g^{-1}$. Thus, appropriate scan rates have been calculated and applied in the cyclic voltammetry measurements. For iodide-based systems, a high redox peak on the positive electrode can be observed. Rubidium hydroxide is characterized by more equal potential ranges for both electrodes. Such findings are in accordance with EQCM electrochemical tests (**Fig. S7**). It needs to be highlighted that in EQCM measurements, both electrodes have been studied with the same scan rate in order to record a reliable EQCM response. Moreover, to collect many experimental points, a wide potential range has been applied. In the case of the 0.1 $mol \cdot L^{-1}$ KI electrolytic solution depicted in **Fig. S7C,** one may notice slightly more resistive character of the CV curves. Limited charge propagation results from the application of a very wide potential range, where a non-equilibrium state has been reached.

Tab. S3 Potential ranges for cyclic voltammetry recorded for YP-50F carbon and 0.1 $mol \cdot L^{-1}$ electrolytic solutions

Electrolytic solution	Negative electrode potential *vs.* SHE, V	Positive electrode potential *vs.* SHE, V	ΔU, V
3-electrode Swagelok® cell			
NaI	-0.8 ÷ -0.3	-0.3 ÷ 0.0	0.8
KI	-0.8 ÷ -0.2	-0.2 ÷ 0.0	0.8
RbI	-0.9 ÷ -0.4	-0.4 ÷ -0.1	0.8
RbOH	-0.6 ÷ -0.3	-0.3 ÷ 0.2	0.8
3-electrode EQCM cell			
NaI	-1.2 ÷ 0.0	0.0 ÷ 0.4	1.60
KI	-1.5 ÷ -0.06	-0.06 ÷ 0.3	1.80

RbI	-1.20 ÷ 0.24	0.24 ÷ 0.55	1.75
RbOH	-1.4 ÷ 0.0	0.0 ÷ 0.4	1.80

The data in **Tab. S3** represents the experimentally determined potential ranges. However, in the Swagelok® system, all electrolytes have been tested only up to a cell voltage of 0.8 V, for comparison purposes. In the EQCM application, the presented potential ranges directly correlate with the curves shown within the manuscript. What needs to be kept in mind is that the observed phenomena are valid for a ±0.3 V voltage shift. However, such a wide potential window allows better screening of the electrostatic attractions between specific ion adsorption/desorption and co-ion transport from the porous structure of the electrode. The application of high potential amplitudes in EQCM measurements has been described in the literature as an element that allows noticeable mass transfer differences to be observed.

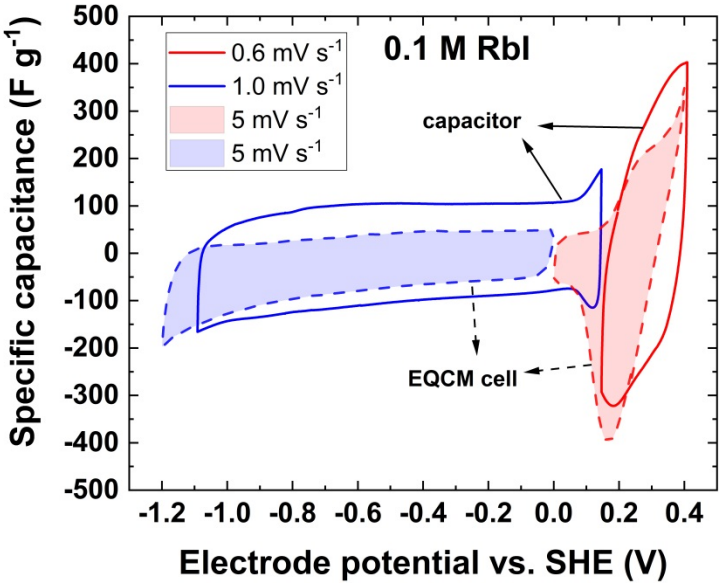

Fig. S8 Cyclic voltammetry profiles in Swagelok® and EQCM setups (electrode: YP-50F; electrolyte: 0.1 mol·L^{-1} RbI)

Fig. S8 depicts the wide potential range cyclic voltammetry for 0.1 mol·L^{-1} RbI recorded in a symmetric Swagelok® cell and 3-electrode EQCM setup. What is proved by this comparison is that both systems work similarly in terms of the stored capacity and separate electrode potentials.

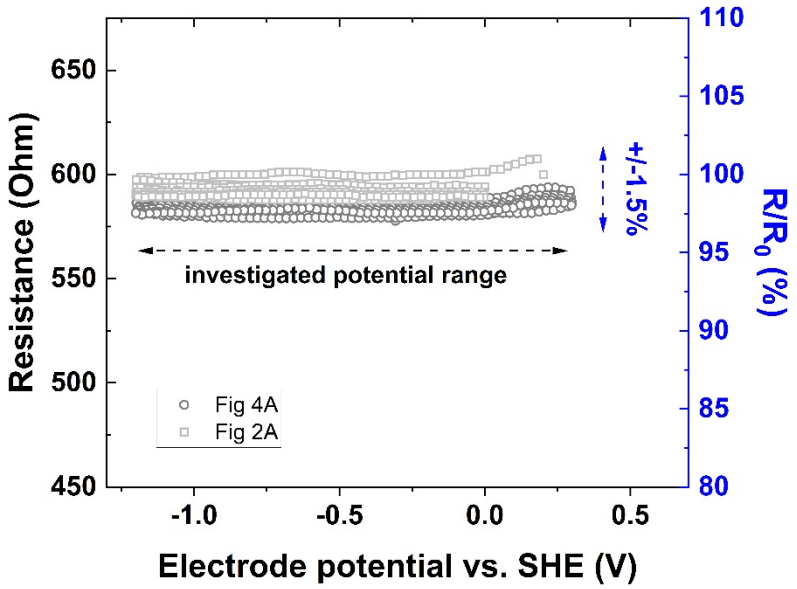

Fig. S9 Resistance profile during cyclic voltammetry in the EQCM cell

In **Fig. S9,** resistance profiles as a function of time during cyclic voltammetry are depicted. These profiles are correlated with the electrochemical curves presented in **Figs. 2A** and **4A**. The overall resistance change during those experiments varies by less than 2%. Resistance fluctuations are in accordance with the current flowing through the system.

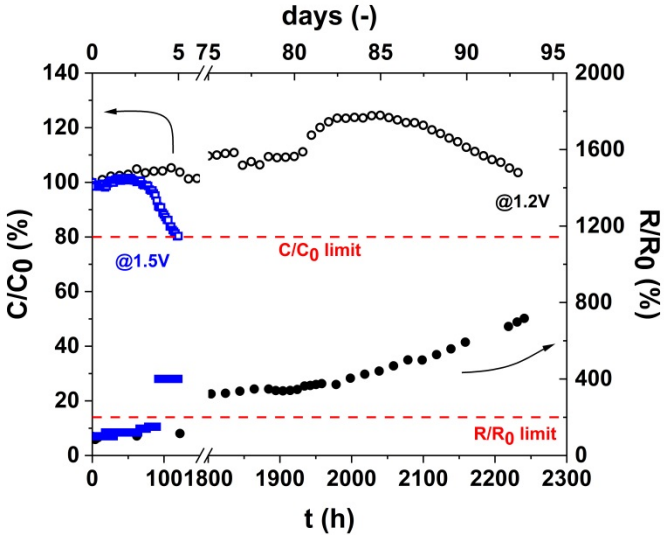

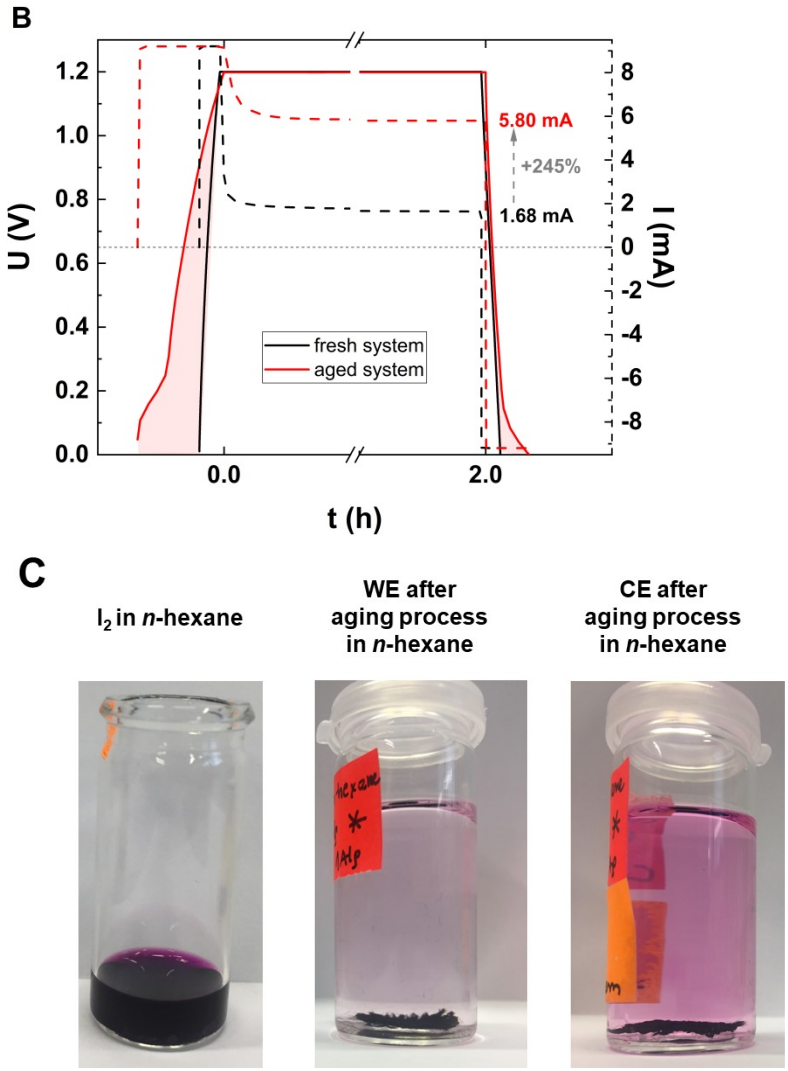

Fig. S10 Aging in a Swagelok® cell (electrode: Kynol 507-20; electrolyte: 1.0 mol·L^{-1} KI) at 1.5 V and 1.2 V: A) relative capacitance and relative resistance as a function of time [10]; B) voltage and current profiles for fresh and aged cells at 1.2 V; C) n-hexane eluate after washing the electrodes subjected to aging process

Fig. S10 presents aging data for 1.0 mol·L^{-1} KI in a symmetric Swagelok® cell. The data recorded at 1.5 V are reprinted from [10]. Both the capacitance and resistance profiles clearly show that the system operating at elevated voltage, i.e., 1.5 V, is not stable over time, and the performance fade is recorded after 120 h at a constant polarization, a process called *floating*. When a limited voltage is applied, 1.2 V, the system is capable of

operating for up to 2000 h without a 20% decrease in the specific capacitance. However, as the energy storage mechanism is based on a dual mechanism, with redox reactions at the positive electrode and electrical double-layer formation at the negative electrode, a constant resistance increase is observed. However, considering an increase in resistance up to 200%, the system operating at 1.2 V exhibits a much longer operation time than that at 1.5 V. Fluctuations recorded for the capacitance profile may result from temperature variations during the experiment and moreover, from activation of redox processes and shift of redox potentials over time due to a local, superficial pH change. **Fig. S10B**, on the other hand, shows a constant polarization curve for the system operating at 1.2 V. The black curve represents the first *floating* cycle, and the red curve represents the last cycle recorded. It can be observed that the leakage current increases by approx. 250%; however, it is still characterized by a plateau. From the filling under the curve for the aged cell, an energy difference might be observed in comparison to the fresh cell. The first remark is that energy efficiency is lower after 2000 h at a constant polarization. Furthermore, the discharge profile exhibits a tail at a low voltage, which is also confirmed in [72]. This result suggests that the equilibrium state of iodide/iodine redox reactions changes over time. This feature is not a drawback of the system. Only if the reactions exceed safety limits, they will cause iodate precipitation and drastic failure of the system (as observed at 1.5 V). However, what is worth highlighting is the fact that a system capable of performing *floating* for more than 200-300 h has not been previously presented in the literature. **Fig. S10C** stands as an analytical proof that iodine is trapped in the electrode porosity after electrochemical operation. At the beginning, the electrodes have been thoroughly washed with deionized water, then dried and studied by N_2 adsorption. After adsorption tests, the same process has been repeated, however, with *n*-hexane as a solvent. Change of color to pinkish/violet clearly demonstrates I_2 strongly bond to carbon surface, as the first step washing, degassing in a vacuum and N_2 analysis do not remove it from sample volume. Intensity of the

color is linked to the I_2 concentration (as the same volume of n-hexane has been used for working and counter electrodes). Surprisingly, more I_2 has been found with counter electrode than in working one – proving that $I_2/2I^-$ redox pair is active at the both electrode/electrolyte interfaces, altering its equilibrium state. Moreover, it is a proof that counter electrode also contains iodide-based species and their activity/presence on the surface cannot be neglected.

To sum up, in the full-cell system one cannot simplify ion fluxes to be separated by charge towards either working or counter electrode. $I_2/2I^-$/carbon specific interactions are forceful and durable and do not require external polarization.

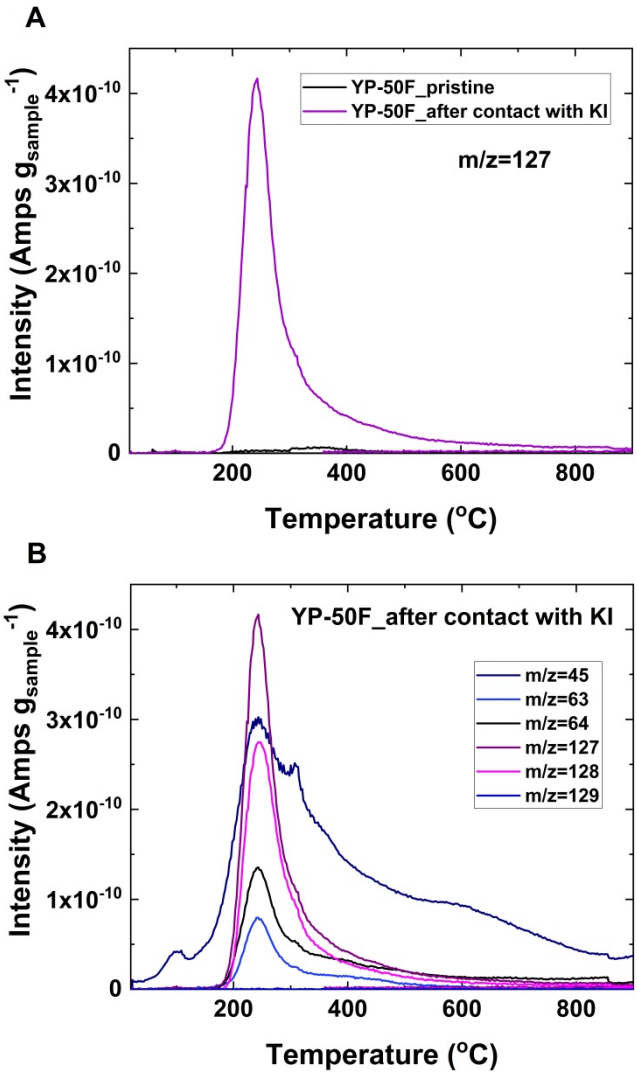

Fig. S11 Temperature Programmed Desorption Mass Spectra recorded for YP-50F carbon: A) m/z=127 for pristine sample and one after contact with 1.0 mol L^{-1} KI; B) various m/z spectra for sample after contact with 1.0 mol L^{-1} KI

In order to analytically confirm the iodide/iodine presence in the carbon porosity TPD-MS spectra has been recorded for pristine carbon and one after contact with 1.0 mol L^{-1} potassium iodide solution. YP-50F carbon has been herein selected as the representative carbon, but analogous curves have been recorded for YP-80F and KYNOL 507-20 carbons. **Fig. S11A** compare intensity of m/z peak equal to 127 (corresponding to iodide/iodine flow through MS). Intensity found for sample being in contact with KI is extremely high, comparing to pristine one. Iodide/iodine species has not been calibrated therefore, it is only possible to compare qualitatively samples between themselves – if the same gas/species evolution occurs during thermal decomposition of the sample. As assumed, pristine

carbon does not contain any iodide/iodine species. We are discussing iodide/iodine species not particular one due to the experiment limitation, as one cannot simplify which individuals are evolved from the sample just considering their mass. Ions undergo subsequent ionization process and peak m/z=127 might result from either I^- or I_2^{2-} or even further ionized specimen. However, mass 127 is somewhat related to iodide/iodine species variety. This is why **Fig. S11B** presents various m/z peaks observed at the same temperature (their maximum lies in the same position) indicating that they are compartments of main peak 154 (I_2) or 127 (I^- or I_2^{2-}) as a result of a deep ionization of iodide-based species. Taking into account heating rate, position of temperature peak and the value of universal constant, the energy of carbon-iodine bond has been calculated from TPD. The high value of 139 kJ/mol proves semi-covalent C-I bond.

Given that, beside EQCM technique, other standard analytical methods confirm strong iodide/iodine/carbon specific interactions.